

Cluster Size Analysis of Two-Dimensional Order in Colloidal Gold Nanoparticle Arrays

Beomseok Kim, Marcelo A. Carignano, Steven L. Tripp, and Alexander Wei*

Department of Chemistry, Purdue University, West Lafayette, Indiana 47907-2084

Received May 11, 2004. In Final Form: August 4, 2004

A protocol for cluster size distribution analysis was developed in order to parametrize local two-dimensional (2D) order in a quantitative manner, using mean cluster sizes and fractional hcp cluster formation (f_{hcp}). Cluster size analysis was performed on 2D arrays of Au nanoparticles encapsulated in resorcinarene tetrathiol, which were organized into close-packed films at aqueous interfaces. The degree of monolayer formation and 2D order within the self-assembled nanoparticle arrays was observed to be strongly dependent on the amount and type of electrolyte (chloride and/or citrate) adsorbed on the nanoparticle surface, prior to encapsulation and extraction to the solvent interface. Increasing the concentration of adsorbed electrolyte could promote monolayer film formation but had a variable effect on local 2D order.

Introduction

Colloidal self-assembly has emerged as a leading methodology in the fabrication of nano- and mesoscale materials. An attractive feature of this technique is its ability to promote crystalline order in two or three dimensions, allowing ensemble properties to be correlated with tunable physical parameters such as particle size, interparticle spacing, aspect ratio, and higher-order lattice structure.¹ Examples of nanoparticle 2D and 3D superlattices have increased dramatically in recent years and have yielded novel physical phenomena with exciting potential for chemical sensing,^{2,3} high-density magnetic data storage,⁴ nonlinear and spin-dependent transport,^{5–7} enhanced optical properties such as second-harmonic generation⁸ and surface-enhanced Raman scattering,^{9–13} photonic band gaps at visible and near-infrared wavelengths,^{14,15} and even as templates for mesoporous materials^{16,17} and nanostructured island films.¹⁸

The forces that drive colloidal self-assembly depend on the physical characteristics and surface chemistry of the unit particle as well as on environmental factors. In

particular, particle size and composition determine whether long-range van der Waals (vdW) interactions play an important role in self-organization. For very small nanoparticles, vdW forces are typically at or below thermal energies ($k_{\text{B}}T$), so that self-assembly would be mostly driven by interactions at molecular length scales (e.g., surfactant chain interdigitation).^{19,20} Surfactant-coated nanocrystals with weak vdW interactions can be deposited at submonolayer concentrations onto air–water interfaces and compressed into close-packed 2D arrays in a Langmuir–Blodgett trough^{8,19,21–24} or organized into 3D superlattices by molecular crystal growth techniques.^{25–27} As the particle size increases, the attractive vdW interactions become significant and often dominate the self-organization process; order within the particle arrays then depends on a complex balance of vdW interactions, electrostatic forces, and/or short-range steric repulsion. Dispersions of nanoparticles and colloids subject to long-range vdW interactions have been shown to self-assemble into 2D arrays by simple drop-casting techniques onto wettable or fluid surfaces.^{6,20,28–34} Air–liquid and liquid–liquid

* Corresponding author: e-mail alexwei@purdue.edu.

(1) (a) Collier, C. P.; Vossmeier, T.; Heath, J. R. *Annu. Rev. Phys. Chem.* **1998**, *49*, 371–404. (b) Pileni, M. P. *J. Phys. Chem. B* **2001**, *105*, 3358–3371.

(2) Wohltjen, H.; Snow, A. W. *Anal. Chem.* **1998**, *70*, 2856–2859.

(3) (a) Holtz, J. H.; Asher, S. A. *Nature (London)* **1997**, *389*, 829–832. (b) Asher, S. A.; Alexeev, V. L.; Goponenko, A. V.; Sharma, A. C.; Lednev, I. K.; Wilcox, C. S.; Finegold, D. N. *J. Am. Chem. Soc.* **2003**, *125*, 3322–3339.

(4) Sun, S.; Murray, C. B.; Weller, D.; Folks, L.; Moser, A. *Science* **2000**, *287*, 1989–1992.

(5) Andres, R. P.; Bielefeld, J. D.; Henderson, J. I.; Janes, D. B.; Kolagunta, V. R.; Kubiak, C. P.; Mahoney, W. J.; Osifchin, R. G. *Science* **1996**, *273*, 1690–1693.

(6) Parthasarathy, R.; Lin, X.-M.; Jaeger, H. M. *Phys. Rev. Lett.* **2001**, *87*, 186807.

(7) Black, C. T.; Murray, C. B.; Sandstrom, R. L.; Sun, S. *Science* **2000**, *290*, 1131–1134.

(8) Collier, C. P.; Saykally, R. J.; Shiang, J. J.; Henrichs, S. E.; Heath, J. R. *Science* **1997**, *277*, 1978–1981.

(9) Moody, R. L.; Vo-Dinh, T.; Fletcher, W. H. *Appl. Spectrosc.* **1987**, *41*, 966–970.

(10) Tessier, P. M.; Velez, O. D.; Kalambur, A. T.; Rabolt, J. F.; Lenhoff, A. M.; Kaler, E. W. *J. Am. Chem. Soc.* **2000**, *122*, 9554–9555.

(11) Wei, A.; Kim, B.; Sadtler, B.; Tripp, S. L. *ChemPhysChem* **2001**, *2*, 743–745.

(12) Félidj, N.; Truong, S. L.; Aubard, J.; Lévi, G.; Krenn, J. R.; Hohenau, A.; Leitner, A.; Aussenegg, F. R. *J. Chem. Phys.* **2004**, *120*, 7141–7146.

(13) Genov, D. A.; Sarychev, A. K.; Shalaev, V. M.; Wei, A. *Nano Lett.* **2004**, *4*, 153–158.

(14) Moroz, A. *Phys. Rev. Lett.* **1999**, *83*, 5274–5277.

(15) Braun, P. B.; Wiltzius, P. *Curr. Opin. Colloid Interface Sci.* **2002**, *7*, 116–123.

(16) Johnson, S. A.; Ollivier, P. J.; Mallouk, T. E. *Science* **1999**, *283*, 963–965.

(17) Jiang, P.; Bertone, J. F.; Colvin, V. L. *Science* **2001**, *291*, 453–457.

(18) Jensen, T. R.; Malinsky, M. D.; Haynes, C. L.; van Duyne, R. P. *J. Phys. Chem. B* **2000**, *104*, 10549–10556.

(19) (a) Heath, J. R.; Knobler, C. M.; Leff, D. V. *J. Phys. Chem. B* **1997**, *101*, 189–197. (b) Gelbart, W. M.; Sear, R. P.; Heath, J. R.; Chaney, S. *Faraday Discuss.* **1999**, *112*, 299–307.

(20) Motte, L.; Pileni, M. P. *J. Phys. Chem. B* **1998**, *102*, 4104–4109.

(21) Dabbousi, B. O.; Murray, C. B.; Rubner, M. F.; Bawendi, M. G. *Chem. Mater.* **1994**, *6*, 216–219.

(22) Meldrum, F. C.; Kotov, N. A.; Fendler, J. H. *Chem. Mater.* **1995**, *7*, 1112–1116.

(23) Brown, J. J.; Porter, J. A.; Daghighian, C. P.; Gibson, U. J. *Langmuir* **2001**, *17*, 7966–7969.

(24) Huang, S.; Minami, K.; Sakaue, H.; Shingubara, S.; Takahagi, T. *Langmuir* **2004**, *20*, 2274–2276.

(25) Murray, C. B.; Kagan, C. R.; Bawendi, M. G. *Science* **1995**, *270*, 1335–1338.

(26) Thomas, P. J.; Kulkarni, G. U.; Rao, C. N. R. *J. Phys. Chem. B* **2001**, *105*, 2515–2517.

(27) Talapin, D. V.; Shevchenko, E. V.; Kornowski, A.; Gaponik, N.; Haase, M.; Rogach, A. L.; Weller, H. *Adv. Mater.* **2001**, *13*, 1868–1871.

(28) Harfenist, S. A.; Wang, Z. L.; Alvarez, M. M.; Vezmar, I.; Whetten, R. L. *J. Phys. Chem.* **1996**, *100*, 13904–13910.

(29) Wang, Z. L.; Harfenist, S. A.; Vezmar, I.; Whetten, R. L.; Bentley, J.; Evans, N. D.; Alexander, K. B. *Adv. Mater.* **1998**, *10*, 808–812.

interfaces are especially useful for tuning colloidal interactions and permit self-assembled films to be transferred onto solid surfaces with a high degree of fidelity.^{23,35,36}

Periodic order is widely regarded as an important quality for the collective properties of colloidal arrays and their applications.^{12–15} Order is typically categorized as being long range (crystalline) or short range (local), but its parametrization is largely qualitative in nature. The gray boundary between local and long-range order has created some confusion in their definitions; indeed, many systems which have been described as having long-range order are in reality comprised of close-packed domains with local order. This reveals the need for methods which can provide more precise definitions of order.

The quality of long-range 2D order has been characterized using graphical methods based on autocorrelation functions or static structure factors.^{37–42} These are typically derived from the radial distribution function $g(r)$ (also known as the pair correlation function), which represents particle density at a distance r from a reference site. Here $g(r)$ is defined simply as

$$g(r) \equiv \langle \delta(r') \delta(r' - r) \rangle \quad (1)$$

where $\delta(r)$ is the Kronecker delta function and r' is the position of a given reference particle. Translational 2D order can be illustrated graphically by plotting $g(r)$, using the average periodicity (center-to-center distance) as a unit value. 2D particle arrays with long-range hexagonal order are expected to produce $g(r)$ plots which decay according to an algebraic power law ($r^{-\xi}$, where $\xi \sim 1/3$), whereas particle films with poor translational order should produce $g(r)$ plots that decay exponentially.^{39,40}

Autocorrelation function analyses are best performed using clusters of several thousand particles to minimize perturbations due to data truncation. This precludes a precise description of order at the local level, although parameters of relative order can still be established.^{43,44} Other graphical methods of analysis face similar limitations: for example, the patterns produced by fast Fourier transform (FFT) image analysis depict local order in an intuitive fashion, but in most cases the quality of data does not extend beyond the first order of approximation.

(30) Maye, M. M.; Zheng, W.; Leibowitz, F. L.; Ly, N. K.; Zhong, C. *J. Langmuir* **2000**, *16*, 490–497.

(31) Puentes, V. F.; Krishnan, K. M.; Alivisatos, P. *Appl. Phys. Lett.* **2001**, *78*, 2187–2189.

(32) Lin, X. M.; Jaeger, H. M.; Sorensen, C. M.; Klabunde, K. J. *J. Phys. Chem. B* **2001**, *105*, 3353–3357.

(33) Brown, L. O.; Hutchison, J. E. *J. Phys. Chem. B* **2001**, *105*, 8911–8916.

(34) Yamamuro, S.; Farrell, D.; Humfeld, K. D.; Majetich, S. A. *Mater. Res. Soc. Symp. Proc.* **2001**, *636*, D.10.8.

(35) Kondo, M.; Shinozaki, K.; Bergström, L.; Mizutani, N. *Langmuir* **1995**, *11*, 394–397.

(36) Goldenberg, L. M.; Wagner, J.; Stumpe, J.; Paulke, B. R.; Görnitz, E. *Langmuir* **2002**, *18*, 5627–5629.

(37) (a) Marcus, A. H.; Rice, S. A. *Phys. Rev. Lett.* **1996**, *77*, 2577–2580. (b) Marcus, A. H.; Rice, S. A. *Phys. Rev. E* **1997**, *55*, 637–656. (c) Cui, B.; Lin, B.; Rice, S. A. *J. Chem. Phys.* **2003**, *119*, 2386–2398.

(38) Ramos, L.; Lubensky, T. C.; Dan, N.; Nelson, P.; Weitz, D. A. *Science* **1999**, *286*, 2325–2327.

(39) Terao, T.; Nakayama, T. *Phys. Rev. E* **1999**, *60*, 7157–7162.

(40) Gray, J. J.; Klein, D. H.; Bonnecaze, R. T.; Korgel, B. A. *Phys. Rev. Lett.* **2000**, *85*, 4430–4433.

(41) Kooij, E. S.; Brouwer, E. A. M.; Wormeester, H.; Poelsema, B. *Langmuir* **2002**, *18*, 7677–7682.

(42) Hansen, P. H. F.; Rödnér, S.; Bergström, L. *Langmuir* **2001**, *17*, 4867–4875.

(43) (a) Torquato, S.; Truskett, T. M.; Debenedetti, P. G. *Phys. Rev. Lett.* **2000**, *84*, 2064–2067. (b) Truskett, T. M.; Torquato, S.; Debenedetti, P. G. *Phys. Rev. E* **2000**, *62*, 993–1001.

(44) Shah, P. S.; Novick, B. J.; Hwang, H. S.; Lim, K. T.; Carbonell, R. G.; Johnston, K. P.; Korgel, B. A. *Nano Lett.* **2003**, *3*, 1671–1675.

In this paper we provide a quantitative method for describing local 2D order in self-assembled nanoparticle films based on cluster size distribution analysis. A related method of cluster analysis has been reported by Martin and co-workers, in which locally ordered domains are evaluated by percolation theory for computation of intra-domain correlation functions and lattice spacings.⁴⁵ Here we use cluster size analysis to evaluate local 2D order in colloidal Au nanoparticle films formed by self-organization at air–water interfaces and the influence of electrolyte concentrations on the self-assembly process. The Au nanoparticles are passivated by resorcinarene tetrathiol, whose surfactant properties have been shown to enhance the dispersion and self-assembly of colloidal metal particles in the midnanometer (15–200 nm) size range.^{11,46–53}

Experimental Section

Materials. Tetraundecylresorcin[4]arene tetrathiol was synthesized as previously reported.^{47,49} Colloidal Au particles were purchased from British Biocell International (EM.GC30 or EM.GC40, $\sim 10^{11}$ particles/mL) and characterized by transmission electron microscopy (TEM). The average particle sizes were 34 ± 2 nm ($N = 1007$) or 35 ± 3 nm ($N = 1165$). Carbon-coated Cu TEM grids were purchased from Ted Pella, Inc., and used as supplied. The resorcinarene-encapsulated nanoparticles were handled in silanized glassware (SiliClad, Gel-Est) to minimize surface adsorption. High-purity water with a measured resistivity above $18 \text{ M}\Omega\cdot\text{cm}$ was obtained using an ultrafiltration system (Milli-Q, Millipore) and passed through a $0.22 \mu\text{m}$ filter to remove particulate matter.

General Procedures. Self-Assembly of Resorcinarene-Encapsulated Au Nanoparticle Monolayers. Aqueous suspensions of colloidal Au particles with fixed electrolyte concentrations were prepared by first treating the commercial solutions with a mixed-bed ion-exchange resin (Amberlite MB-3, Mallinckrodt) for 30 min and then reintroducing electrolytes in a controlled fashion (see Results and Discussion). The ion-exchange resin was thoroughly washed with deionized water before use. The pH of the colloidal solutions was 3–4 after treatment with ion-exchange resin but increased to 7.0–7.4 after addition of salt or surfactant, suggesting the release of adsorbed hydroxide ions from the nanoparticle surfaces. Resorcinarene-encapsulated nanoparticles were prepared by vigorously mixing colloidal suspensions (1 mL) with 1 mM solution of surfactant in THF (1 mL), which produced a homogeneous pink solution. Addition and vigorous mixing of toluene (1 mL) resulted in a separation of organic and aqueous layers; in most cases, a dark film of encapsulated Au nanoparticles could be observed at the biphasic interface. The organic layer was removed, and the nanoparticles were washed twice more with toluene (1 mL each) to extract THF and excess surfactant. The Au nanoparticles were drawn up in a silanized glass pipet, then drained, and carefully redeposited onto a clean air–water interface in a silanized test tube and allowed to stand at room temperature for 60 min. Unless otherwise mentioned, the nanoparticle films were deposited onto Formvar-coated Cu grids by Langmuir–Schaefer transfer using a pair of forceps, then dried in air.

(45) Martin, J. E.; Wilcoxon, J. P.; Odinek, J.; Provencio, P. *J. Phys. Chem. B* **2000**, *104*, 9475–9486.

(46) Stavens, K. B.; Pusztay, S. V.; Zou, S.; Andres, R. P.; Wei, A. *Langmuir* **1999**, *15*, 8337–8339.

(47) Kim, B.; Tripp, S. L.; Wei, A. *J. Am. Chem. Soc.* **2001**, *123*, 7955–7956.

(48) Wei, A.; Kim, B.; Pusztay, S. V.; Tripp, S. L.; Balasubramanian, R. *J. Inclusion Phenom. Macrocycl. Chem.* **2001**, *41*, 83–86.

(49) (a) Balasubramanian, R.; Xu, J.; Kim, B.; Sadtler, B.; Wei, A. *J. Dispersion Sci. Technol.* **2001**, *22*, 485–489. (b) Balasubramanian, R.; Kim, B.; Tripp, S. L.; Wang, X.; Lieberman, M.; Wei, A. *Langmuir* **2002**, *18*, 3676–3681.

(50) Tripp, S. L.; Pusztay, S. V.; Ribbe, A. E.; Wei, A. *J. Am. Chem. Soc.* **2002**, *124*, 7914–7915.

(51) Tripp, S. L.; Dunin-Borkowski, R. E.; Wei, A. *Angew. Chem., Int. Ed.* **2003**, *42*, 5591–5593.

(52) Liu, J.; Ong, W.; Kaifer, A. E. *Langmuir* **2002**, *18*, 5981–5983.

(53) Kim, B.; Balasubramanian, R.; Pérez-Segarra, W.; Wei, A.; Decker, B.; Mattay, J. *Supramol. Chem.* **2004**, *16*, in press.

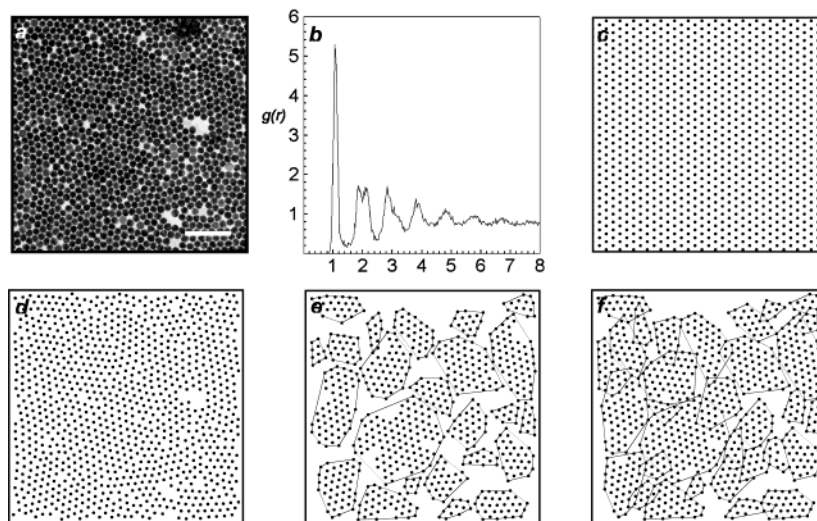


Figure 1. Cluster size distribution analysis of colloidal Au nanoparticle array, extracted to the air–water interface using resorcinarene tetrathiol. Nanoparticles were treated with ion-exchange resin prior to extraction. (a) TEM image of self-assembled nanoparticle film (34 ± 2 nm, $N = 1002$, scale bar = 200 nm); (b) $g(r)$ plot derived from nanoparticle 2D array, as a function of average periodicity; (c) crystalline template with periodicity and lattice site diameters defined by the position and line width of the primary $g(r)$ peak; (d) map of particle centroids; (e) nonoverlapping hcp clusters within 2D array; (f) partially overlapping hcp clusters within nanoparticle 2D array. Domain boundaries are drawn to guide the eye.

TEM Characterization and Image Analysis of Au Nanoparticle Monolayers. TEM analysis was performed with a Philips EM-400 using an accelerating voltage of 80 kV. In most cases, images were acquired at 46 000 \times ; magnifications at 20 000 \times or higher were calibrated using crystals of beef catalase ($d = 8.75$ nm). Negatives containing Au nanoparticles ($N = 650$ – 1000) were scanned at 1200 dpi (Perfection 1200U Photo Scanner, Epson) and digitized using a size analysis program (SigmaScan Pro 5.0, SPSS); images were saved in tagged-image file (TIF) format. All particle size analyses were performed prior to additional image processing.

Autocorrelation and Cluster Size Distribution Analyses. To obtain the centroids of individual Au particles for autocorrelation analyses, the gray scale intensities of each image were first normalized according to a histogram stretch. Regions containing partial bilayers were digitally excised to reveal continuous monolayers of nanoparticles. Particles within the image were then selected by applying an overlay and optimizing the intensity threshold. Overlapping particle edges were separated by treating the images with several digital filters; in some cases, conjoined particles were separated manually. Pixel coordinates were then recorded as data files and used to determine centroid coordinates and radial distribution functions; codes were programmed using MatLab 6.5.

Cluster size distribution analysis for a given particle monolayer was performed by first defining a hexagonal crystalline lattice, whose periodicity was derived from the primary peak of the corresponding $g(r)$ plot. This served as a template for identifying hexagonal close-packed (hcp) clusters of particles within the nanoparticle film. The template was rotated in 1 deg increments about a given centroid, for a total of 60 analyses per particle. Clusters were obtained by correlating neighboring particle centroids with contiguous crystalline lattice sites, whose threshold for inclusion could be adjusted by an extrinsic parameter Δ . Particle clusters with $N > 6$ were recorded for size distribution analysis, with an option to remove overlapping subsets. Programs for generating $g(r)$, lattice templates, and cluster size distributions are available under Supporting Information.

Results and Discussion

Nanoparticle Self-Assembly at the Air–Water Interface. Colloidal nanoparticles dispersed in aqueous solutions are typically stabilized by negative electrical double layers, whose repulsions are dictated by solution ionic strength and by the adsorption of anions onto the particle surface.⁵⁴ Introducing chemisorptive nonionic surfactants can displace most but not necessarily all

adsorbates, such that a residual surface charge remains. Incomplete passivation by hydrophobic surfactants can thus render nanoparticles amphipathic and lead to their confinement at the aqueous interface, as noted in several earlier studies on the self-assembly of mesoscopic latex and functionalized silica particles.^{35,55–57} In addition, electrostatic interactions often have influential but complex contributions toward interparticle potentials and can promote either kinetic aggregation or electrostatic repulsion. The nature and concentration of the adsorbed electrolytes are thus of considerable practical importance, yet most suspensions of charge-stabilized metal nanoparticles contain poorly defined mixtures of electrolytes, with less than desirable consequences for reproducible self-assembly.

To establish control over electrostatic potential, aqueous dispersions of Au nanoparticles were preconditioned with an ion-exchange resin to remove electrolytes, which were then reintroduced in defined amounts.⁵⁸ Standardizing electrolyte concentrations in this manner improved reproducibility in the dispersion behavior of nanoparticles from different batches and provided a means for correlating adsorbate concentrations with 2D order in the self-assembled Au nanoparticle films (see below). The effect of ion exchange on nanoparticle extraction and film formation is unmistakable: attempts to extract 35 nm Au particles to the water–toluene interface using resorcinarene tetrathiol without any prior treatment resulted in emulsion formation, whereas preconditioning with ion-exchange resin for 10–30 min permitted the extraction of nanoparticles to the solvent interface and their subsequent self-organization into 2D arrays (see Figure 1a).

(54) (a) Israelachvili, J. *Intermolecular and Surface Forces*, 2nd ed.; Academic Press: New York, 1992. (b) Evans, D. F.; Wennerström, H. *The Colloidal Domain: Where Physics, Chemistry, Biology, and Technology Meet*, 2nd ed.; Wiley-VCH: New York, 1999.

(55) Pieranski, P. *Phys. Rev. Lett.* **1980**, *45*, 569–572.

(56) Beck, C.; Hartl, W.; Hempelmann, R. *Angew. Chem., Int. Ed.* **1999**, *38*, 1297–1300.

(57) (a) Hansen, P. H. F.; Bergström, L. *J. Colloid Interface Sci.* **1999**, *218*, 77–87. (b) Hansen, P. H. F.; Malmsten, M.; Bergenstahl, B.; Bergström, L. *J. Colloid Interface Sci.* **1999**, *220*, 269–280.

(58) Enüstün, B. V.; Turkevich, J. *J. Am. Chem. Soc.* **1963**, *85*, 3317–3328.

It is worth mentioning that longer exposure times to ion-exchange resin (12 h) allowed the resorcinarene-encapsulated nanoparticles to be completely extracted into the organic phase (toluene/THF), even without the aid of phase-transfer salts.⁴⁹ Here the surface charge on these particles can be assumed to be minimal. However, deposition of the fully extracted Au nanoparticles onto aqueous interfaces, followed by evaporation of the organic solvent and Langmuir–Schaefer film transfer, resulted in multilayered aggregates. This indicates that as the residual organic film is concentrated, kinetic agglomeration driven by the nanoparticles' strong vdW attractions supersedes reversible self-organization at the solvent interface. Surface charge is therefore important for promoting monoparticulate film formation, as it confines amphiphathic nanoparticles to the aqueous interface.

2D order analysis was performed on a self-organized array of colloidal Au nanoparticles (34 ± 2 nm) encapsulated in resorcinarene tetrathiol, which had been extracted to the air–water interface from a solution containing minimal electrolyte (see Figure 1a).⁴⁷ Both FFT analysis (not shown) and autocorrelation analysis (see Figure 1b) provided qualitative indications of good local order; in addition to generating several harmonics, the $g(r)$ plot revealed a characteristic doublet centered about $r = 2$.^{39–41} However, the $g(r)$ trace fitted poorly to an algebraic decay envelope and was too steep to suggest any possibility of long-range order. Indeed, Au nanoparticle films of varying quality produced $g(r)$ plots with vaguely similar decay functions (see below), precluding their direct comparison for assessing subtle differences in 2D order.

Cluster size distributions enabled a quantitative analysis of local 2D order in the nanoparticle films. Several criteria are necessary to establish inclusion of a given particle within a hcp cluster domain: (1) a minimum of two nearest-neighbor particles within the same cluster; (2) a local correlation angle $\psi = 60^\circ$; (3) an established center-to-center distance between particle centroids; and (4) an adjustable parameter Δ to accommodate the variance in particle diameter and ellipticity, yet maintain a well-defined standard for hcp clustering. The latter two criteria are readily defined by the primary peak in the $g(r)$ plot ($r = 1$), whose peak width at half-maximum provides an appropriate coefficient of variance for monodispersity in particle size and shape. These parameters were used to produce a hexagonal array of lattice sites with radius of acceptance Δ (see Figure 1c).⁵⁹ The crystalline lattice was then used as a template and applied to each particle centroid to identify hcp clusters within the 2D arrays. Starting from a minimal nucleus of seven particles, clusters were determined by the inclusion of centroids within the radius of acceptance following the criteria above.

Clusters obtained in this fashion were prioritized by size and then further refined to minimize redundancy in particle count due to overlapping domains. Refinements were performed in two ways: (i) calculation of cluster size distributions with no overlap between domains, in which smaller, partially overlapping clusters were removed from the analysis (see Figure 1e), and (ii) calculation of cluster size distributions using a predefined threshold of overlap (see Figure 1f). In this work, we set an upper limit of 30% overlap between any two clusters. The first refinement method has the advantage of eliminating redundancy,

but at the expense of discounting a small fraction of particles belonging to hcp clusters. The second method is more comprehensive in coverage but is skewed toward smaller cluster populations. For this reason, we applied both number-averaged and weight-averaged cluster sizes (M_n and M_w , respectively) as figures of merit for describing 2D order and for quantitative comparisons between 2D arrays prepared under different conditions.

Cluster size analysis on the 2D nanoparticle array in Figure 1 revealed a number of hcp domains, the largest ones containing up to 100 particles. In the case of nonoverlapping clusters, M_n and M_w were calculated to be 30.3 and 44.9, respectively; in the case of partially overlapping clusters, the mean values were found to be 29.7 and 42.3. Cluster analysis also showed that the majority of particles in the self-assembled film were members of an ordered domain; the fraction of particles belonging to an hcp cluster (f_{hcp}) in the nonoverlapping case was determined to be 0.73, whereas that in the partially overlapping case was determined to be 0.83. The minor differences between the two cases suggest that cluster size distribution analysis using either refinement method could adequately describe the quality of hcp ordering within the 2D arrays. However, analyses based on nonoverlapping clusters require fewer assumptions, which is desirable for making quantitative comparisons of 2D order.

While cluster analysis can provide useful insights into 2D order, it assumes monolayer formation and does not address the issue of multilayers in self-assembled nanoparticle films. Monoparticulate films are desirable from both a practical and theoretical perspective, as periodic 2D lattices can be correlated with collective physical states.¹³ Digital image analysis of the self-assembled nanoparticle film over a sufficiently large sample area indicated a significant fraction of multilayer coverage (approximately 15.4% over $64 \mu\text{m}^2$). We considered that monolayer formation could depend on the nanoparticles' surface wetting properties, which in turn could be modulated by the adsorption of controlled quantities of electrolyte species.

The Role of Adsorbed Electrolyte in Au Nanoparticle Array Formation. To better define the role of ionic adsorbates in the self-organization of the Au nanoparticle arrays, a set of experiments were performed in which electrolytes were introduced under controlled conditions to colloidal suspensions (see Table 1). Preconditioned gold nanoparticles (35 ± 3 nm) were dispersed in fixed concentrations of NaCl and trisodium citrate (Na_3Cit), the latter as an associative electrolyte to evaluate the relative importance of surface charge. Nanoparticles were then extracted to the solvent interface with resorcinarene tetrathiol, collected and redeposited onto a fresh air–water interface, and transferred onto carbon-coated Cu TEM grids as described in the Experimental Section. Several samples prepared under identical conditions produced arrays of similar quality, so variations due to experimental error have been assumed to be small.

Two qualitative trends were immediately apparent upon inspection of the TEM images (see Figure 2, column I). First, nanoparticles extracted from solutions of low ionic strength ($I < 5$ mM) were observed to self-assemble into films with relatively large hcp clusters but tended to contain a significant fraction of multilayers (see Table 1). Second, nanoparticles extracted from solutions of higher ionic strength ($I > 7$ mM) could self-assemble into colloidal films with essentially monolayer thickness, but often at some expense of 2D order. Autocorrelation functions also provided a qualitative indication of order; 2D arrays of

(59) Values for Δ (calculated in pixels) are dependent on the quality of the $g(r)$ plot from which they are derived. A typical value for Δ in this study is 16 pixels, which corresponds to 18–20% of the periodicity.

Table 1. Colloidal Gold Nanoparticle Arrays after Extraction from Electrolyte Solutions^a

array	particle count (N) ^b	NaCl (mM)	Na ₃ Cit (mM)	ionic strength (mM) ^c	hcp clusters, no overlap			hcp clusters, partial overlap ^d			multilayer (%)
					M_n	M_w	f_{hcp}	M_n	M_w	f_{hcp}	
1	901	0	0	0	21.4	28.5	0.64	22.4	28.2	0.74	12.9
2 ^e	n/a	0	0.25	1.5							27.6
3	879	1.63	0.25	3.13	19.6	26.5	0.63	18.4	24.5	0.74	35.3
4 ^e	n/a	3.23	0	3.23							28.4
5	918	1.63	0.50	4.63	24.6	32.0	0.59	21.2	28.3	0.74	15.8
6	715	4.75	0.25	6.25	15.3	17.1	0.49	14.7	16.6	0.57	9.5
7	797	0	1.22	7.32	15.5	18.8	0.55	15.4	18.3	0.62	5.3
8	654	4.75	0.50	7.75	12.5	14.3	0.27	12.3	14.0	0.28	1.6
9	923	1.63	1.22	8.95	20.5	26.1	0.62	20.8	25.4	0.77	0.8
10	706	4.75	0.75	9.25	17.8	21.6	0.52	16.5	20.3	0.61	1.8

^a Gold nanoparticles (35 ± 3 nm) were preconditioned with MB-3 ion-exchange resin for 30 min before exposure to added electrolytes and encapsulation with resorcinarene tetrathiol. ^b Number of centroids taken from TEM image. ^c Prior to nanoparticle extraction. ^d The threshold for overlap between clusters was 30%. ^e Cluster size analysis was not attempted on these samples.

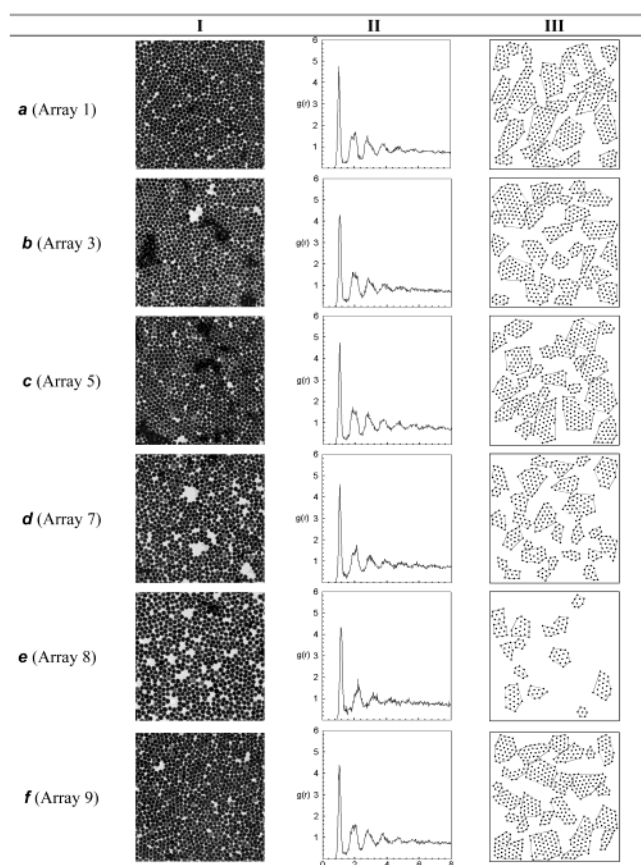


Figure 2. TEM images (column I), $g(r)$ plots (column II), and size distribution analyses of nonoverlapping hcp clusters (column III) taken from 2D arrays of Au particles (35 ± 3 nm) extracted from various electrolyte solutions: (a) NaCl = 0 mM, Na₃Cit = 0 mM; (b) NaCl = 1.63 mM, Na₃Cit = 0.25 mM; (c) NaCl = 1.63 mM, Na₃Cit = 0.50 mM; (d) NaCl = 0 mM, Na₃Cit = 1.22 mM; (e) NaCl = 4.75 mM, Na₃Cit = 0.50 mM; (f) NaCl = 1.63 mM, Na₃Cit = 1.22 mM.

nanoparticles exposed to low electrolyte concentrations produced $g(r)$ plots with a discernible doublet centered about $r = 2$ (see Figure 2, column II). However, fitting the $g(r)$ functions to either algebraic or exponential decay envelopes did not reveal any clear trends relating electrolyte concentration to 2D order.

Cluster size distribution analyses were then performed for additional insights (see Figure 2, column III). The mean cluster sizes provided a simple but quantitative metric for comparing the quality of 2D order between gold nanoparticle arrays formed under different self-assembly conditions. As expected, the mean cluster sizes calculated

under conditions of zero overlap were very similar to those calculated using partially overlapping clusters (see Table 1). It is worth noting that the hcp clusters formed from these nanoparticles are smaller than those produced in Figure 1, possibly because of their higher size polydispersity. The relative differences in 2D order within this series are assumed to be due primarily to changes in electrolyte concentrations.

The mean cluster sizes provided a sufficient degree of precision to assess subtle differences in quality between nanoparticle films. One surprising result revealed by this quantitative method of analysis was the lack of correlation between mean cluster size and the ionic strength of the colloidal solution prior to extraction. Particles extracted from a solution containing relatively high levels of NaCl and Na₃Cit ($I = 8.95$ mM, array 9) could self-organize into films with comparable hcp cluster sizes and f_{hcp} values as particles extracted from solutions of low ionic strength ($I < 5$ mM, arrays 1 and 3). This was encouraging, as higher ionic strength clearly had a beneficial impact on monolayer film formation. However, hcp cluster formation appeared to be quite sensitive to the balance of electrolytes; for example, particles suspended in solutions with high ionic strength but different ratios of NaCl to Na₃Cit (arrays 7 and 8) produced smaller mean cluster sizes as a result of kinetic aggregation. The loss of 2D order was likewise reflected in the lower f_{hcp} values, which was greater than 0.60 for relatively well-ordered nanoparticle films but on the order of 0.50 or less for films populated with small hcp clusters. This illustrates the complex influence of the adsorbed electrolytes on interparticle attraction and repulsion, which precludes any simple conclusions regarding the relationship between nanoparticle surface charge and 2D ordering at air–water interfaces.

Another example of the complex interplay between surface charge and nanoparticle 2D array formation at the solvent interface is provided by the degree of monolayer film structure as a function of initial ionic strength. Films comprised of nanoparticles extracted from solutions with low salt content were patchy and contained much higher percentages of multilayers (see Table 1, arrays 2–4) than those extracted from solutions of either minimal ionic strength (array 1) or with ionic strength above 5 mM (arrays 6–10). In contrast, particles extracted at high ionic strength were much more likely to produce films of uniform thickness; in the case of array 9, the monolayer film structure extended for many thousands of square microns, with defects caused primarily by shear forces during film transfer (see Figure 3). Here electrostatic and short-range steric repulsion operated synergistically

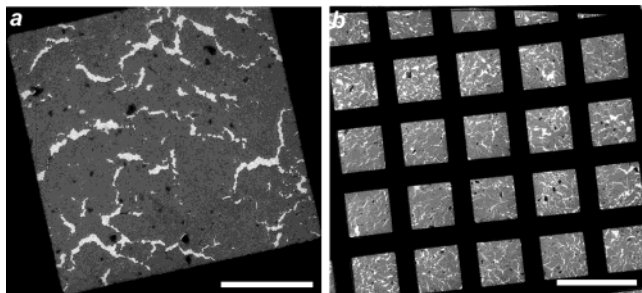


Figure 3. TEM images of extended 2D arrays of colloidal gold particles extracted from aqueous solutions containing 1.22 mM NaCl and 1.63 mM Na₃Cit and then redeposited onto a fresh air–water interface (array 9): (a) scale bar = 20 μm; (b) scale bar = 100 μm. Cracks within the array were assumed to have formed during Langmuir–Schaefer film transfer.

to reduce kinetic aggregation and promote thermodynamic self-organization at the air–water interface.

Free electrolytes are well-known to modulate the electrostatic double layers surrounding particles in aqueous dispersions, which determine their long-range repulsive screening potentials.⁵⁴ On the other hand, adsorbed electrolytes contribute directly toward the surface charge of the colloid, which affects their wetting behavior at the solvent interface. In our system, nanoparticle self-assembly is performed on the surfaces of deionized water, so local electrostatic effects are presumed to be dominant. Our studies show that increased electrolyte adsorption promotes monoparticulate film formation simply by increasing nanoparticle adhesion to the aqueous interface.

Particle wetting can also have a moderating effect on interparticle pair potentials: Bergström and co-workers have proposed that the degree of immersion of particles confined at the air–water interface alters their effective Hamaker constants and hence their rate of spontaneous aggregation.⁵⁷ This notion appears to be in general accord with our observations, but the sensitivity of 2D ordering to specific ratios of adsorbed electrolytes indicates additional electrokinetic effects which remain to be addressed.

In summary, our studies demonstrate how cluster size distributions can be used to provide a quantitative measure of local 2D order. These were used to evaluate the influence of adsorbed electrolytes at different concentrations, which produced subtle but discernible differences in the formation of hcp clusters within the self-assembled Au nanoparticle arrays. This method of cluster analysis may have utility in the characterization of ordered domains within other 2D periodic structures.

Acknowledgment. The authors gratefully acknowledge financial support from the National Science Foundation (BES-0228143, CHE-0243496, ECS-0210445), Mr. Seungseok Oh for valuable assistance with MatLab programming, and Prof. Igal Szleifer for helpful discussions.

Supporting Information Available: Computer programs for radial distribution functions and cluster size distribution analysis, written for MatLab 6.5. This material is available free of charge via the Internet at <http://pubs.acs.org>.

LA0488351